Phys. Rev. Applied **13**, 054070 (2020) - Published 27 May 2020. Q1

Parametric generation of subharmonics in a composite multiferroic resonator

D.A. Burdin,[1] D.V. Chashin,[1] N.A. Ekonomov,[1] V.L. Preobrazhenskii,[2] S.N. Gordeev,[3] and Y.K. Fetisov[1]

[1]*MIREA – Russian Technological University, Moscow 119454, Russia*

[2]*Prokhorov General Physics Institute RAS, Moscow 119991, Russia*

[3] *Department of Physics and Centre for Nanoscience & Nanotechnology, University of Bath, BA2 7AY, U.K.*

(Received …..

Parametric generation of subharmonics in a composite multiferroic resonator has been observed and investigated. The resonator has the form of a disk and contains two mechanically coupled layers, one of which is amorphous ferromagnet FeBSiC and the other piezoelectric lead zirconate-titanate. The resonator was placed inside two planar electromagnetic coils with orthogonal axes. A static magnetic field of 0-100 Oe was applied parallel to the plane of the resonator. The resonator was excited in the frequency range f = 9-10 kHz by either a harmonic magnetic field with an amplitude of up to 5 Oe generated by one of the coils, or a harmonic electric field with an amplitude of up to 500 V/cm applied to the piezoelectric layer. When the pump field was above a certain threshold, generation of a subharmonic of half-frequency (f/2) was observed for three different excitation methods. The first two employed either the direct magnetoelectric effect or the converse magnetoelectric effect, while in the third a transformer system was utilised. The subharmonic was generated in a limited range of pump frequencies and its amplitude was a nonlinear function of both the pump-field amplitude and the strength of static magnetic field. A theory of parametric generation of the subharmonic in a multiferroic resonator has been developed, taking into account the magnetoacoustic nonlinearity of the ferromagnetic layer of the structure and excitation of acoustic resonances near the pump and subharmonic frequencies. The theory qualitatively describes the main characteristics of the subharmonic generation.

DOI: PACS numbers(s):

I. INTRODUCTION

Magnetoelectric (ME) effects in composite multiferroic heterostructures have been extensively studied in recent decades due to prospects of creating highly sensitive sensors of magnetic field [1-3], new devices for radio-signal processing [4-6], elements of magnetic memory switchable by voltage [7-9], and autonomous power sources for microelectronic devices [10]. ME effects in planar ferromagnetic-piezoelectric (PM-PE) structures result from a combination of magnetostriction in the PM layer and piezoelectricity in the PE layer due to the mechanical coupling of the layers [11,12]. The effects manifest themselves either as a change in polarization of the structure in an external magnetic field (the direct effect) or as a change in magnetization, when an electric field is applied (the converse effect). In particular, when a magnetic field is applied, magnetostriction of the FM layer causes it to expand on contract. This deformation is transmitted to the PE layer, which, due to the piezoelectric effect, generates an electric voltage. In practice, ME effects are usually investigated by affecting a heterostructure with an alternating magnetic (h) or electric (e) field and recording the response of the structure at the same frequency (f) [13]. The magnitude of the direct ME effect is characterized by the magnetoelectric coefficient $\alpha_E = v/(a_p h)$, where v is the amplitude of the voltage generated by the structure, a_p is the thickness of the PE layer. In turn, the magnitude of the converse ME effect is characterised by the coefficient $\alpha_B = \delta B / e$, where δB is the change in magnetic induction of the FM layer.

To date, the linear ME effects in heterostructures of different compositions and different shapes have been studied quite well. It is shown that the efficiency of both direct and converse ME transformations depends strongly on materials of the layers [12,14,15] as well as strength and orientation of external magnetic and electric fields [16,17]. For excitations with variable fields, the ME conversion efficiency increases by 2-3 orders of magnitude due to a sharp rise of mechanical deformations when the frequency of the excitation field coincides with the frequency of an acoustic resonance in the structure [18,19]. As a result of research in the last two decades, the maximum efficiency of the direct ME effect was increased from ~ 20 mV/(cm Oe) to ~ 20 kV/(cm Oe) [20].

A number of nonlinear ME effects have also been observed for a large-field excitation of the heterostructures. Nonlinear effects are shown to occur due to the nonlinear dependence of magnetostriction λ of the FM layer on static magnetic field H, nonlinear dependence of the magnetization of the FM layer M on deformation S, and nonlinear dependence of deformation S of the PE layer on electric field E. Among the discovered nonlinear ME effects are frequency doubling and generation of higher harmonics of voltage [21] or magnetization [22], voltage generation with the sum and difference frequencies when the structure is excited by two different magnetic or electric harmonic fields [23-25], suppression of ME hysteresis in heterostructures [26], occurrence of bistability in a ME acoustic resonator [27], paramet-

ric amplification of a signal when the heterostructure is pumped by an electric field with double frequency [28, 29].

In the present work a nonlinear effect of generation of the half-frequency subharmonic in a ferromagnet-piezoelectric planar heterostructure, excited by a harmonic magnetic or harmonic electric field, is experimentally observed. It is shown that the subharmonic generation arises due to the magnetoacoustic nonlinearity of the ferromagnetic layer and when both the excitation frequency and its subharmonic are close to the frequency of an acoustic resonance in the heterostructure. Note that generation of subharmonics is used in parametric optical generators [30]. Generation of subharmonics was observed in nonlinear magnetoacoustic ferrite [31] and antiferromagnetic [32] resonators.

The first part of the work describes the multiferroic FM-PE heterostructure used in the experiments and various regimes of subharmonic generation. The second part shows the results of experimental studies of subharmonic generation when the heterostructure is excited by an alternating magnetic or electric field. Then a theory of parametric generation of subharmonics in FM-PE heterostructures is described. The obtained results are discussed in the next part of the work. Finally, the main results and conclusions of the work are summarised.

II. COMPOSITE FERROMAGNET-PIEZOELECTRIC RESONATOR AND MEASUREMENT TECHNIQUES

In the experiments, a disk resonator (see Fig. 1) of radius R = 8 mm was used. It contained an FM layer of amorphous ferromagnet FeBSiC (Metglas 2605SA1, produced by Metglas®, Inc. USA [33]) of thickness a_m = 20 μm and a PE layer of lead zirconate titanate $PbZr_{0.52}Ti_{0.48}O_3$ (PZT-19, produced by Elpa Research Institute, Moscow, Russia [34]) of thickness a_p = 200 μm. The amorphous FM was chosen because it possesses a rather high saturation magnetostriction of $\lambda_S \approx 23 \cdot 10^{-6}$ and a small saturation field $H_S \approx 100$ Oe thus facilitating observation of nonlinear effects. The surface of the PZT disk was coated with 2 μm thick Ag-electrodes and poled perpendicular to the plane in a constant electric field of 15 kV/cm. The PZT's piezomodule was $\eta_{31} \approx -5.2$ C/m^2. The layers of ferromagnet and piezoelectric were bonded to each other with a layer of Loctite epoxy adhesive (~4 μm thick) under pressure. The resonator was placed inside flat electromagnetic coils with mutually perpendicular axes inserted into each other as shown in Fig. 1.

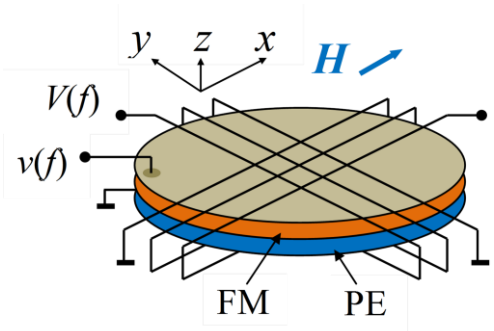

FIG. 1. Schematic diagram of the FM-PE resonator with excitation and receiving coils subjected to a static magnetic field *H*.

The inner coil had a cross-section of 40 mm^2 and contained N_1 = 200 turns of 0.2 mm diameter wire. The outer coil had a cross-section of 80 mm^2 and contained N_2 = 220 turns of the same wire. A static magnetic field *H* was applied parallel to the plane of the structure along the *x*-axis.

A schematic diagram of the experimental setup is shown in Fig. 2. Agilent 35210 generator was used to generate ME effects by applying voltage *V* from it either to the excitation coil (to study the direct ME effect) or to the PZT layer electrodes (to study the converse ME effect). Static magnetic field *H* = 0-120 Oe was produced by Helmholtz coils of 20 cm in diameter, which were powered by Agilent E3634 DC source. Magnetic field was measured by LakeShore 421gaussmeter with 0.1 Oe accuracy. The waveform of generated voltage *v*(*t*) was recorded by Tektronix TDS3032B oscilloscope, and FFT Network Analyzer SR770 was used to observe voltage spectra *v* (*f*). The setup enabled us to record characteristics of the generated response for different values of *f*, *h*, *e* and *H*.

The measurements were performed in three different regimes.

- In the first regime, the resonator was excited by an alternating magnetic field. The schematic diagram for this case is shown in Fig. 2. Voltage *V* (*f*) was applied to the inner coil, that created in the sample an ac magnetic field of amplitude up to *h* = 5 Oe and frequency *f* = 0.1-12 kHz directed parallel to the field *H* and the plane of the sample along the *x*-axis. The amplitude and waveform of voltage *v*(*f*) generated due to the direct ME effect between the electrodes on the top and bottom surfaces of the PZT layer was recorded.
- In the second regime, the resonator was excited by an alternating electric field. Voltage *V*(*f*) was applied to the electrodes of the PZT layer, producing a variable electric field of the amplitude up to *e* = 500 V/cm, directed along the *z*-axis. Voltage *v(f)* generated by the inner coil due to the converse ME effect was recorded.

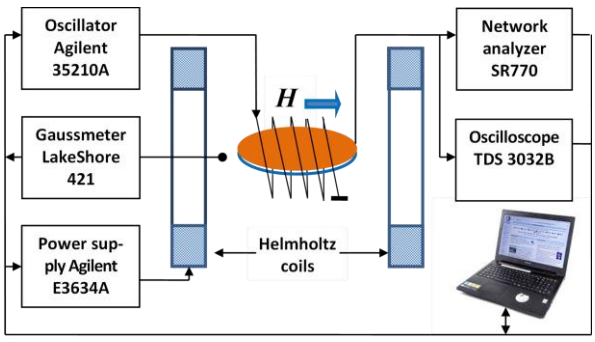

FIG. 2. Block diagram of the setup for studying parametric generation upon excitation of the resonator by magnetic field.

- In the third regime, the resonator was excited by an alternating magnetic field created by the inner coil when voltage *V*(*f*) from the generator was applied to it. The generated by the outer coil voltage *v(f)*, which is proportional to the amplitude of magnetoacoustic oscillations in the structure, was recorded in this case. The orthogonal orientation of the coil axes provided minimal direct electromagnetic interference.

III. EXPERIMENTAL RESULTS

A. Parametric generation in the case of direct magnetoelectric effect

Figure 3 shows the amplitude-frequency (a) and phase-frequency (b) responses of the resonator for the direct ME effect (regime 1). The resonator was excited by a magnetic field of small amplitude, h = 1 Oe, while the frequency of the excitation field was scanned, and the amplitude v and phase φ of the voltage generated by the PZT layer of the structure were recorded. Two resonances, one with central frequency $f_1 \approx 5.56$ kHz and quality factor $Q_1 \approx 22$ and the other with central frequency $f_2 \approx 9.96$ kHz and $Q_2 \approx 40$ were observed. It will be shown below that these resonances correspond to an excitation of lower modes of bending vibrations of the disk structure. Near the resonance frequencies, the phase of the generated signal (see Fig. 3b) changes by ~180 degrees.

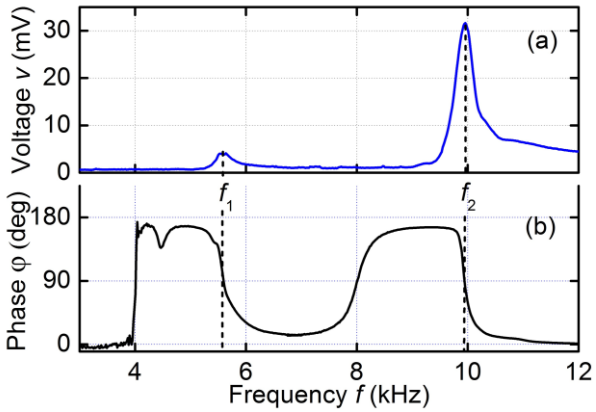

FIG. 3. Amplitude-frequency (a) and phase-frequency (b) responses of FM-PE resonator for h = 1 Oe and H = 18 Oe.

Frequency spectra of the measured voltage (see Fig. 4) clearly show the occurrence of parametric generation. When the resonator is excited by a pump magnetic field of small amplitude h = 1 Oe at frequency f_p = 10 kHz, only a component of amplitude v_p at this frequency is observed in the spectrum. An increase in the excitation field amplitude above a certain threshold h_{th} results in a generation of a subharmonic of amplitude v_s with frequency $f_s = f_p/2$ that corresponds to a half of the excitation frequency.

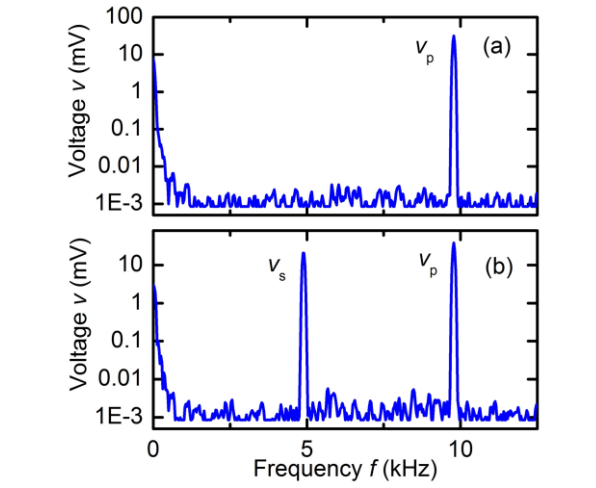

FIG. 4. Frequency spectra of generated voltage due to direct ME effect for H = 18 Oe, when: (a) field h = 1 Oe is below threshold; (b) field h = 4 Oe is above threshold.

Figure 5 shows the subharmonic amplitude as a function of frequency of pump field f_p in a static magnetic field H = 45 Oe for different amplitudes h of pump field. Initially, when the threshold amplitude $h_{th} \approx 2$ Oe is reached, the subharmonic appears only when the structure is excited at frequency f_p = 9.96 kHz. Then, with increasing h, the frequency region within which the subharmonic is generated, gradually expands up to $f_p \approx$ 9.5-10.5 kHz for h = 5 Oe. In the latter case, the amplitude of the subharmonic rises sharply near the boundaries of the range and decreases monotonically with increasing frequency within the range. There is a small hysteresis between the up and down sweeps.

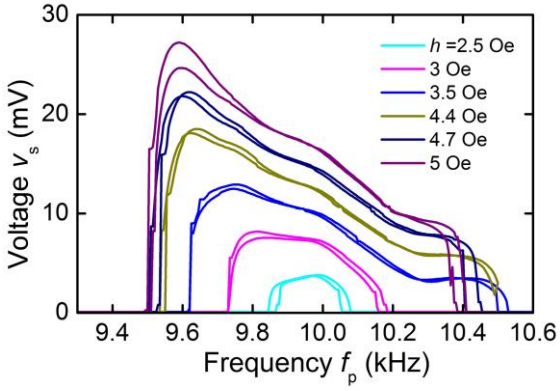

FIG. 5. Subharmonic amplitude as a function of pump field frequency for direct ME effect and different amplitudes of alternating magnetic field h in static field H = 45 Oe.

Figure 6 shows dependences of the subharmonic amplitude on the magnitude of static magnetic field H for different amplitudes of excitation magnetic field with frequency f_p = 9.7 kHz. Upon reaching the threshold amplitude $h_{th} \approx 2$ Oe, the subharmonic first appears at $H_{m1} \approx 48$ Oe. Then, with increasing h, the field region at which the subharmonic is generated gradually expands, reaching $H \approx$ 20-110 Oe for h=5 Oe. In the latter case, the amplitude of the subharmonic

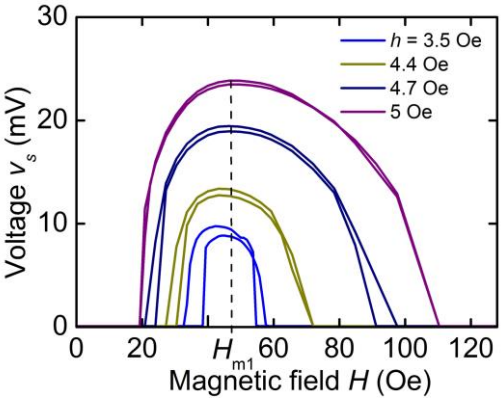

FIG. 6. Subharmonic amplitude as a function of static field for direct ME effect for different pump field amplitudes h and f_p = 9.7 kHz.

is maximum in the center of the range and decreases monotonically near its boundaries.

Figure 7 shows the subharmonic amplitude as a function of pump field amplitude h at f_p = 9.7 kHz for different static fields H. It can be seen that with an increase in h, the amplitude of the subharmonic increases, first sharply and then more slowly. A subsequent decrease in h results in a hysteretic behaviour: the subharmonic amplitude is larger for decreasing than for increasing h. In accordance with Fig. 6, an increase in H first increases the subharmonic's amplitude but then decreases it when H becomes greater than 50 Oe.

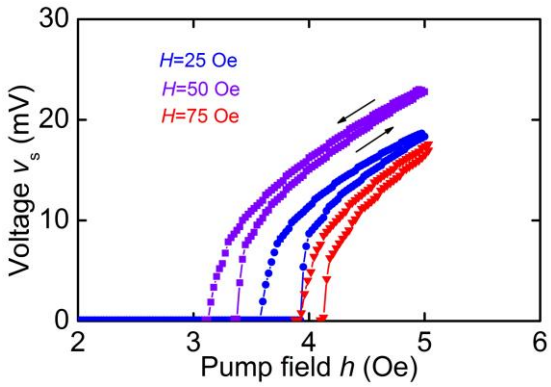

FIG. 7. Dependences of subharmonic amplitude on amplitude of excitation field for f_p = 9.7 kHz and different static fields H in the case of direct ME effect.

B. Parametric generation in the case of converse magnetoelectric effect

In the case of the converse ME effect (regime 2), when the resonator is excited by an electric field e applied to the PZT layer and the voltage generated by the internal coil is recorded, the frequency and phase responses are similar to those shown in Fig. 3. With an increase in the amplitude of pump electric field above the threshold value $e_{th} \approx 50$ V/cm, a generation of the subharmonic with a half of the excitation frequency $f_s = f_p / 2$ is observed.

Figure 8 shows dependences of the subharmonic amplitude v_s on frequency f_p of the pump electric field for different excitation amplitudes e in a fixed field H = 30 Oe. It can be seen that near the threshold $e_{th} \approx 50$ V/cm, the subharmonic appears at approximately the same frequency $f_p \approx 9.95$ kHz as in regime 1. As the amplitude of the pump field increases, the region of frequencies where the subharmonic is excited, gradually grows and shifts downward to occupy the range from 9.35 kHz to 9.9 kHz at e = 500 V/cm. In the latter case, the subharmonic amplitude v_s is approximately constant within the range and decreases sharply as f_p approaches its boundaries.

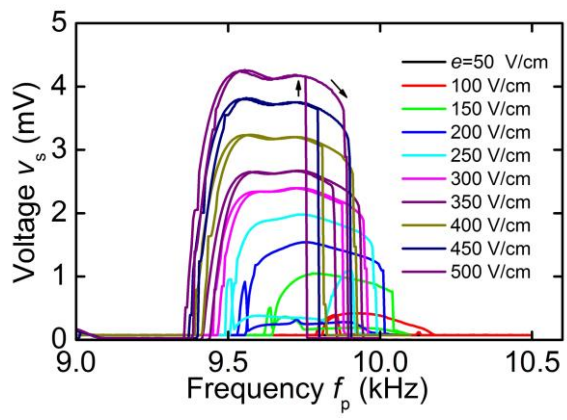

FIG. 8. Subharmonic amplitude vs pump field frequency at H = 30 Oe and different amplitudes of field e in the case of converse ME effect.

Figure 9 shows dependences of the subharmonic amplitude v_s on field H at frequency f_p = 9.7 kHz of the pump field for a range of excitation amplitudes e. It can be seen that v_s initially grows with H, reaching a maximum at $H_{m2} \approx 25$ Oe, then it decreases, tending to zero due to a progressive saturation of the FM layer. The maximum amplitude of the subharmonic increases with the amplitude of excitation field e.

Dependences of the subharmonic amplitude v_s on pump filed amplitude e at f_p = 9.7 kHz for a range of fields H are given in Fig. 10. For e above the threshold $e_{th} \approx 140$ V/cm, the curves first rise abruptly but then grow almost linearly with e. There is a small hysteresis between the curves for increasing and decreasing e. The subharmonic amplitude also depends on the strength of static field H. In agreement with Fig. 9, maximum v_s first increases with H and then decreases for H >25 Oe.

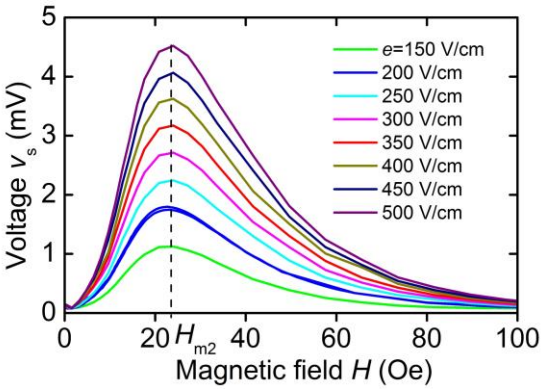

FIG. 9. Subharmonic amplitude as a function of static magnetic field for pump frequency f_p = 9.7 kHz and different amplitudes of alternating electric field e in the case of converse ME effect.

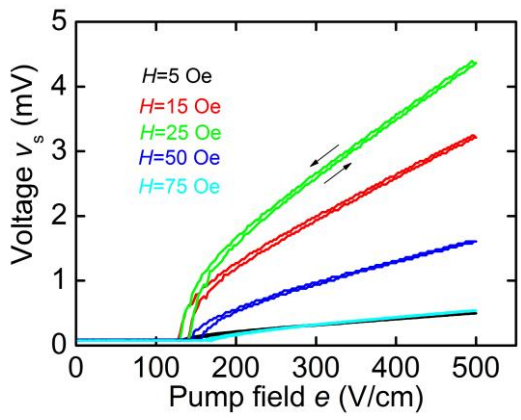

FIG. 10. Subharmonic amplitude as a function the excitation field amplitude for f_p = 9.7 kHz and different magnetic fields H in the case of converse ME effect.

C. Parametric generation in the case of transformer effect

When the resonator is excited by the magnetic field of the inner coil and detection of the magneto-acoustic oscillations performed by measuring the generated magnetic field with the outer coil (regime 3), the amplitude-frequency and phase-frequency responses are similar to those shown in Fig. 3. Parametric generation of the half-frequency subharmonic is observed when the amplitude of the excitation field is above the threshold. Fig. 11 shows dependence of the subharmonic amplitude on frequency of pumping field for a range of pumping amplitudes h when static field H = 25 Oe is applied. The generation of the half-frequency subharmonic is first observed for an excitation with $f_p \approx 9.93$ kHz when the excitation amplitude is just above $h_{th} \approx 2$ Oe. With increasing h the subharmonic is generated in a larger and larger range of excitation frequencies, up to 9.64-10.1 kHz for h = 5 Oe. The low-frequency edge of the curves has a greater slope than the high-frequency edge. There is a small hysteresis between the up and down sweeps.

Figure 12 shows the subharmonic amplitude as a function of static field H for excitation frequency f_p = 9.7 kHz and different amplitudes of excitation field h. As h reaches the threshold value $h_{th} \approx 2.5$ Oe, the subharmonic first appears at magnetic field $H \approx 48$ Oe. As h increases, the range of magnetic fields H supporting generation of the subharmonic extends up to 13-120 Oe for h = 5 Oe. Within the range, the amplitude of the subharmonic first increases with H, reaching its maximum at $H_{m3} \approx 35$ Oe and then decreases. The maxima of the curves shift slightly to higher H values for $h < 3.5$ Oe.

Figure 13 shows dependences of the subharmonic amplitude on excitation field h at pumping frequency f_p = 9.7 kHz and for various static fields H. The curves first show an abrupt growth just above h_{th} but then monotonously increases with h. A significant hysteresis is observed between the sweeps up and down. Both the threshold value and the subharmonic amplitude are non-monotonous functions of field H.

The frequency of bending oscillations of the resonator can be estimated using the formula for oscillations of a free disk of radius R and thickness a. The frequencies of the lower bending modes are given by relation [35]

$$f = k_{ns} \frac{a}{2\pi R^2} \sqrt{\frac{Y}{12\rho(1-\gamma^2)}}, \qquad (1)$$

where k_{ns} is the mode-dependent coefficient, n is the number of nodal diameters, l is the number of nodal circles, ρ is density, Y is the Young 's modulus and $\gamma \approx 0.3$ is the Poisson's ratio. For the two lower modes with one nodal circle, k_{ns} is equal either to $k_{10} = 9.076$ or $k_{11} = 20.52$. The effective values of the Young's modulus and density can be estimated as $Y = (Y_p a_p + Y_m a_m)/(a_p + a_m)$ and $\rho = (\rho_p a_p + \rho_m a_m)/(a_p + a_m)$, respectively. Here, the subscripts "p" and "m" correspond to the PE layer and the FM layer, respectively. Substituting $a = a_p + a_m = 220$ μm, R = 8 mm, $Y_p = 7 \cdot 10^{10}$ N/m^2, $Y_m = 18.6 \cdot 10^{10}$ N/m^2, $\rho_p = 7.7 \cdot 10^3$ kg/m^3 and $\rho_m = 8.2 \cdot 10^3$ kg/m^3 into Eq. (1), one can get frequencies of the lower flexural modes as $f_1 \approx 4.84$ kHz and $f_2 \approx 10.94$ kHz, which are in satisfactory agreement with the experimental values (see Fig. 3).

Thus, in all excitation modes of the structure, when the threshold amplitude of the excitation magnetic or electric field is exceeded, parametric generation of the half-frequency subharmonic is observed. Our experimental results show that the subharmonic characteristics have a complex dependence on frequency of excitation field f_p, strength of static magnetic field H and amplitude of excitation magnetic h or electric e fields. A detailed theoretical analysis of these characteristics is given below.

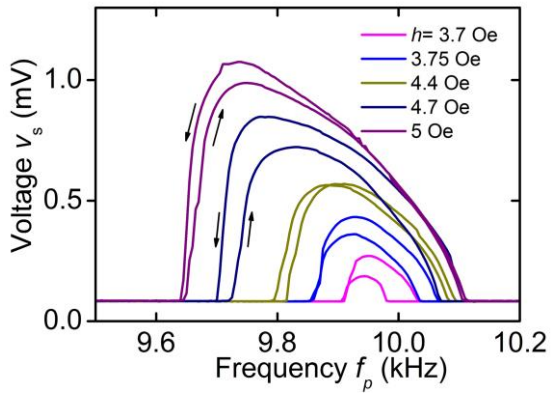

FIG. 11. Subharmonic amplitude vs pump frequency for different amplitudes of alternating magnetic field and H =25 Oe measured in the transformer regime.

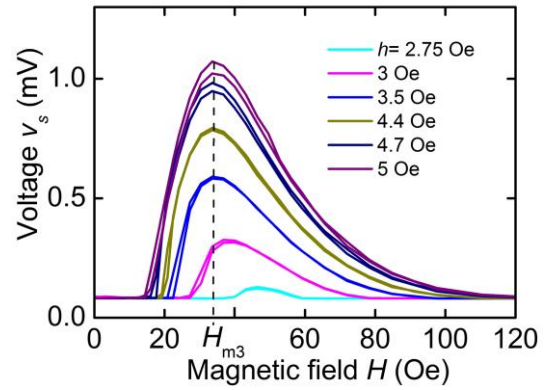

FIG. 12. Subharmonic amplitude vs static magnetic field for different pump field amplitudes at frequency f_p = 9.7 kHz measured in the transformer regime.

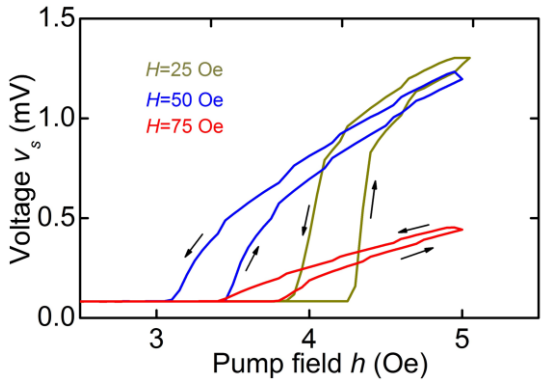

FIG. 13. Subharmonic amplitude as a function the excitation field amplitude at f_p=9.7 kHz for different fields H measured in the transformer regime.

IV. THEORY OF PARAMETRIC GENERATION OF SUBHARMONICS

The results of the experiments exhibit parametric interaction of resonant acoustic modes of the structure excited by either an alternating magnetic or electric field. The mode interaction is a result of acoustic nonlinearity of the magnetic layer of the composite structure and so is imposed to the elastic subsystem by the magnetic subsystem. This mechanism is particularly effective near points of spin reorientation [36], especially in magnetically soft materials, like the amorphous magnetic alloy in the investigated heterostructure.

To describe the observed parametric phenomena, we write the potential energy of the system as a sum of nonlinear elastic F_e, piezomagnetic F_{pm}, and piezoelectric F_{pe} components:

$$F = \int d\vec{r}\left(F_e + F_{pm} + F_{pe}\right), \tag{2}$$

where $F_e = \sum_k \frac{1}{k!} \hat{C}^{(k)} \hat{u}^{(k)}$, $F_{pm} = 2b\vec{M}_0(\hat{u}\hat{\chi})\vec{h}$, $F_{pe} = \vec{e}(\hat{d}\hat{u})$, $\hat{u}^{(k)}$ is the strain tensor, $\hat{C}^{(k)}$, is the κ-th order tensor of elastic moduli, b is the magnetostriction constant, $\hat{\eta}$ is the tensor of piezomoduli, $\hat{\chi}$ is the magnetic susceptibility tensor, M_0 is the equilibrium magnetization, $\vec{h}$ and $\vec{e}$ are the vectors of the alternating magnetic and electric fields, respectively.

Substituting the variable deformations in the form of expansion in terms of the normal modes of elastic oscillations $\hat{u}(\vec{r},t) = \sum_p q_p(t)\hat{u}_p(\vec{r})$, the system in question can be reduced to a system of interacting oscillators:

$$F = \sum_{p,m,n} \frac{1}{3!} C_{pnm} q_p q_m q_n + \sum_{p,m,n,l} \frac{1}{4!} C_{pmnl} q_p q_m q_n q_l + \\ + \sum_p (\vec{\eta}_p \vec{h} + \vec{\xi}_p \vec{e}) q_p + \sum_p \frac{1}{2} C_p q_p^2, \tag{3}$$

where $C_p = \int_V d\vec{r}\,\hat{C}^{(2)}\hat{u}_p^2$, $C_{pmn} = \int_V d\vec{r}\,\hat{C}^{(3)}\hat{u}_p\hat{u}_m\hat{u}_n$, $C_{pmnl} = \int_V d\vec{r}\,\hat{C}^{(4)}\hat{u}_p\hat{u}_m\hat{u}_n\hat{u}_l$, $\vec{\eta}_p = \int_{V_m} d\vec{r}\,2b\vec{M}_0(\hat{u}_p\hat{\chi})$, $\vec{\xi}_p = \int_{V_p} d\vec{r}\,\hat{e}\hat{u}_p(\vec{r})$, and q_p are the amplitudes of the normal modes.

The equations of motion for the amplitudes of normal modes can be obtained in the form of standard Lagrange equations:

$$\frac{\partial}{\partial t}\left(\frac{\partial L}{\partial \dot{q}_p}\right) = \frac{\partial L}{\partial q_p}. \tag{4}$$

Here the potential component of the Lagrange function is given by Eq. (3) and its kinetic part can be written as $T = \sum_p \frac{1}{2} M_p \left(\frac{\partial \dot{q}_p}{\partial t}\right)^2$, where M_p is the effective mass associated with the normal mode $\omega_p^2 = C_p / M_p$.

In the experimental conditions described above, the resonance mode q_p, which was employed for parametric excitation, did not exhibit any noticeable nonlinearity, whereas for the subharmonic mode q_s a substantial negative nonlinear frequency shift was observed, as is clearly seen in Fig. 8 and Fig. 11. This makes it possible to use the linear approximation while describing an excitation of the pumping mode by alternating fields:

$$\frac{\partial^2 q_p}{\partial t^2} + \omega_p^2 q_p + 2\delta_p \frac{\partial q_p}{\partial t} + g_p(t) = 0, \tag{5}$$

where δ_p is the mode attenuation coefficient and $g_p(t) = \frac{1}{M_p}\left(\vec{\eta}_p\vec{h}_p(t) + \vec{\xi}_p\vec{e}(t)\right)$ is the variable excitation force.

In the equation of motion for the subharmonic mode we take into account its parametric interaction with the pumping mode and its cubic nonlinearity, which causes nonlinear frequency shift and restricts the amplitude of the parametric oscillations:

$$\frac{\partial^2 q_s}{\partial t^2} + \omega_s^2 q_s + 2\delta_s \frac{\partial q_s}{\partial t} + D_{ps} q_p q_s + \frac{1}{3} D_{sss} q_s^3 = 0, \tag{6}$$

where δ_s is the attenuation coefficient of the subharmonic mode, $D_{ps} = C_{pss}/M_s$, $D_{sss} = C_{sss}/M_s$ and M_s is the effective mass related to the mode frequency $\omega_s^2 = C_s / M_s$. Note that the quadratic nonlinearity of the subharmonic mode can also contribute to the nonlinear frequency shift in the second order of perturbation theory. For simplicity, it can be assumed that the amplitude of the subharmonic is sufficiently small, so that its effect on the pumping can be neglected. For a harmonic excitation field $g_p(t) = g_p \exp(i\Omega_p t) + c.c.$, the steady state solution of the coupled equations (5) and (6) can be written in the form of harmonic oscillations: $q_p = A_p \exp(i\Omega_p t) + c.c.$ and $q_s = A_s \exp(i\Omega_p t/2) + c.c.$ with frequencies Ω and $\Omega/2$, respectively.

The stationary solutions for the pump amplitude A_p and its subharmonic A_s can be obtained from Eqs (5) and (6) in the following form:

$$|A_p|^2 = \frac{g_p^2}{(2\delta_p\Omega_p^2)^2 + (\Delta\omega_p^2)^2}, \tag{7}$$

$$|D_{sss}A_s|^2 = \sqrt{D_{ps}^2|A_p|^2 - (\Omega_p\delta_s)^2} + \Delta(\omega_s^2). \tag{8}$$

where $\Delta\omega_p^2 = \omega_p^2 - \Omega_p^2$ and $\Delta\omega_s^2 = \omega_s^2 - (\Omega_p/2)^2$ indicate the frequency mismatches for the pump frequency and its subharmonic, respectively. In Eq. (8), the non-linear frequency shift has the negative sign $D_{sss} < 0$, in agreement with the experimental results for bistability [26].

In our experiments, the regime of parametric generation is controlled by the amplitude and frequency of the pump magnetic or electric field. Therefore, it is convenient to exclude the nonlinear interaction parameter D_{ps} from Eq. (8). When the pump frequency is tuned exactly to the resonance, i.e. $\Delta\omega_p^2 = 0$, and $\omega_p = 2\omega_s$, the parameter D_{ps} can be expressed in terms of the threshold value g_{pc} of pump amplitude, leading to:

$$\left|A_p^c\right|^2 = g_{pc}^2/(2\delta_p\omega_p)^2 \qquad (9)$$

The threshold condition requires the subharmonic amplitude A_s in equation (7) to be equal to zero, which under the mentioned above constraints leads to the equality

$$D_{ps}^2\left|A_p^c\right|^2 = (\delta_s\omega_p)^2. \qquad (10)$$

Substituting D_{ps} from Eq. (10) into Eq (8) and taking into account Eq. (9), the solution for the subharmonic amplitude can be obtained as:

$$\left|D_{sss}A_s^2\right|\frac{1}{\omega_s^2} = 1 - \nu_p^2\left(\frac{\omega_p}{2\omega_s}\right)^2 + \frac{1}{Q_s}\left(\frac{\omega_p}{2\omega_s}\right)\sqrt{\frac{P}{\nu_p^2 + (1-\nu_p^2)Q_p^2} - \nu_p^2}\,, \qquad (11)$$

where $P = (g_p/g_{pc})^2$ is the supercriticality parameter, $w_p = \Omega_p/\omega_p$ is the normalised pump frequency and $Q_{s,p} = \omega_{s,p}/2\delta_{s,p}$ are the quality parameters of the subharmonic and pumping modes.

Equation (11) describes key characteristics of parametric generation of the subharmonic for all three cases studied in experiments. As an illustration, Fig. 14 shows results of numerical simulations for the dependence of intensity A_s^2 of the generated subharmonic on normalized pump frequency w_p and supercriticality parameter P. The calculations were performed for quality factors Q_s= 22 and Q_p = 40. It can be seen that the shapes of the curves are qualitatively consistent with the experimental results observed in the transformer regime (see Fig. 11). The subharmonic is generated in a limited range of pump frequencies in the vicinity of the main mode. As the pump amplitude increases (i.e. the supercriticality level rises), this band shifts to lower frequency, indicating a nonlinear frequency shift of the subharmonic mode. Thus a rise in the level of supercriticality results in an increase in the subharmonic intensity, in agreement with the experiment.

Figure 15 illustrates the effect of mismatch α between the doubled frequency of the subharmonic mode and frequency of the pump mode (i.e. $\alpha = 2\omega_s/\omega_p \neq 1$) on the dependence of the subharmonic intensity on the normalized pump frequency. Even a small frequency mismatch (α = 1.027) results in a narrowing of the pump frequency range within which the subharmonic generation is observed and a drop in the subharmonic amplitude.

Figure 16 shows the dependence of the subharmonic intensity on the supercriticality parameter P for different w_p including the case of the perfect matching of the pump frequency with the frequency of the main resonance, i.e. α = 1. The curves have a similar shape to those shown in Figs 7, 10 and 13. As soon as a threshold is exceeded, the subharmonic intensity grows (first sharply and then more slowly) with P. The maximum intensity of the subharmonic is achieved in the case of a "rigid" excitation, when the pump frequency is slightly lower than the frequency of the main resonance (w_p = 0.982), which is due to the negative frequency shift in the system.

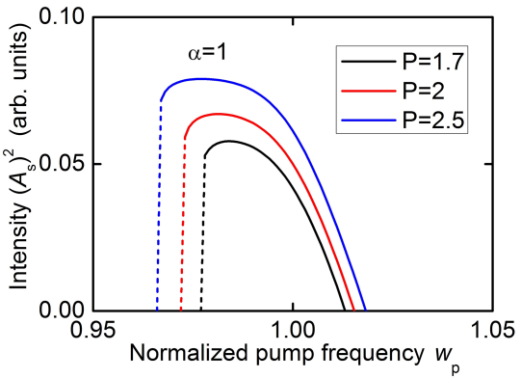

FIG. 14. Dependences of subharmonic intensity on normalized pump frequency for different supercriticality levels when the pump frequency is tuned to the mechanical resonance.

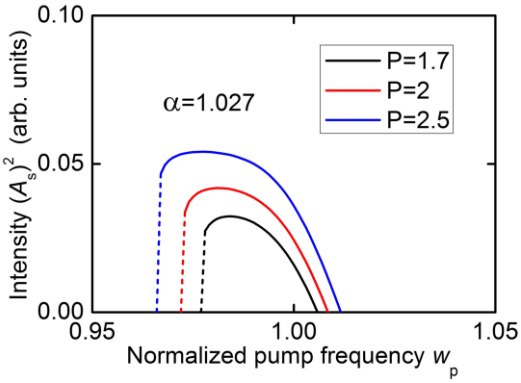

FIG. 15. Dependences of subharmonic intensity on normalized pump frequency for different supercriticality levels in the case of mismatch between pump and resonance frequencies.

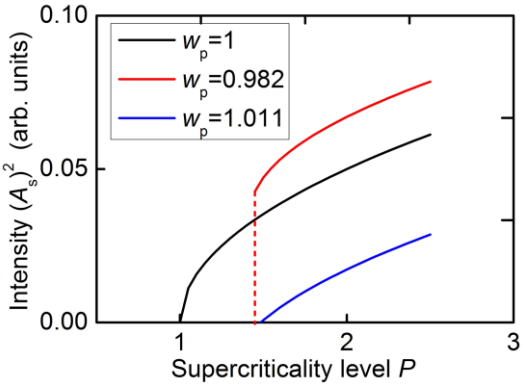

FIG. 16 Dependences of subharmonics intensity on level of supercriticality for different mismatches between doubled frequency of the subharmonic mode and frequency of the pump mode.

V. DISCUSSION OF RESULTS

In our experimental multiferroic resonator, the subharmonic generation occurred in a limited range of pump frequencies adjacent to the second bending mode of the resonator (see Figs 5, 8 and 11). The theory predicts qualitatively the same frequency response (see Figures 14 and 15). In addition, both the experiment and theory reveal an expansion and downward shift of the pump frequency range, in which generation of the subharmonic occurs. Such behaviour of the frequency characteristics is caused by the threshold nature of parametric generation and by a negative shift of the subharmonic's frequency with increasing its amplitude.

The dependence of the subharmonic amplitude (of voltage v_s or of deformation A_s) on magnetic field H is qualitatively different for the three regimes studied, due to differences in excitation and detection of the direct and converse ME effects. When the structure is excited by an alternating magnetic field (the direct ME effect), the subharmonic is generated in a limited range of magnetic fields, the extent of which is determined by the amplitude of the pump magnetic field (see Fig. 6). This is due to the dependence of the amplitude of deformations excited in the structure on the strength of the static magnetic field.

Fig. 17 shows the field dependence of static magnetostrictive deformation $\lambda(H)$ (i.e. magnetostriction) of the FM layer measured by the strain gauge method and the field dependence of piezomagnetic coefficient $\lambda^{(1)}(H) = \partial\lambda / \partial H$ calculated from it. The field dependence of the pump strain amplitude $A_p(H) = \lambda^{(1)}(H)h$ in the structure replicates the field dependence of the piezomagnetic coefficient. The subharmonic generation occurs only when the variable pump strain exceeds the threshold $A_p(H) > A_p^c$ given by Eq.(9). The horizontal dashed line in Fig. 17 corresponds to the piezomagnetic coefficient, at which the variable pump strain in the structure is equal to the threshold value, i.e. $\lambda^{(1)} = \lambda_{th}^{(1)}$. It can be seen from the figure that in this case the subharmonic should be generated only within a limited range of static fields $H_1<H<H_2$. For the amplitude of the pump field h_p producing the threshold deformation $A_p(H) = A_p^c$, the subharmonic generation occurs at field H_m corresponding to the maximum piezomagnetic coefficient for the FM layer of the structure. As the amplitude of the pump field h increases, the region of magnetic fields where the subharmonic is generated also expands. The efficiency of detection of the subharmonic amplitude by the PE layer of the structure is independent of field H, thus resulting in the observed relationship $v_s(H)$ shown in Fig. 6.

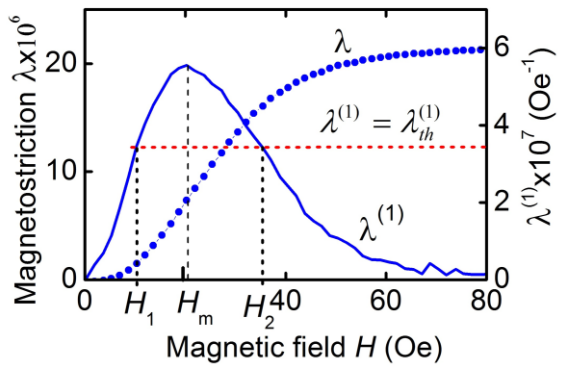

FIG 17 Dependence of magnetostriction λ and piezomagnetic module $\lambda^{(1)}$ on static magnetic field H for the FeBSiC layer.

When the structure is excited by a variable electric field e (the converse ME effect), the deformation in the structure is produced by the PE layer and is independent of the static magnetic field. For deformations exceeding the threshold level $A_p(H) > A_p^c$, oscillations of magnetization with the subharmonic frequency occur at any field H. However, the efficiency of detecting these oscillations depends on H [22], approximately replicating the field dependence of the piezomagnetic coefficient $\lambda^{(1)}(H)$ shown in Fig. 17. As a result, generation of the subharmonic is observed in the entire range of magnetic fields, achieving maximum efficiency at the optimal field H_m=25 Oe and smoothly falling when H decreases or increases, as shown in Fig. 9. In the transformer regime of the subharmonic generation, where deformations in the structure are produced by an alternating magnetic field of the excitation coil, and the amplitude of the generated subharmonic is detected by the second electromagnetic coil, both described above mechanisms operate. As a result, the lower limit of the field interval is clearly formed while the upper limit is less pronounced, as shown in Fig. 12.

The dependence of the amplitude of the generated subharmonic v_s on the amplitude of excitation magnetic h or electric e field in all three regimes was qualitatively the same. When the threshold amplitude of the pump field was exceeded, the harmonic amplitude first abruptly increased but then showed an approximately linear dependence on the field amplitude. A similar dependence is predicted by the developed theory. Hysteresis in dependences of subharmonic amplitude v_s on the pump field amplitude is mainly pronounced when the subharmonic is excited by an alternating magnetic field (Figs 7 and 13) and is due to the magnetic hysteresis of the FM layer.

Finally, let us estimate the efficiency of the subharmonic generation for all three cases. As can be seen from Figs 7, 10, 13 and from Eq. (10), at large excitation field amplitudes, the subharmonic amplitude is approximately a linear function of the pump field amplitude. Thus, for assessing efficiency, it makes sense to use parameters that are similar to those used for assessing the efficiency of field conversion in the linear direct and converse ME effects.

For the linear direct ME effect, the ME conversion coefficient is defined as $\beta_E = u_p / (a_p h)$. Using the results of Fig. 3 and Fig. 4a for a small amplitude of the excitation magnetic field $h \approx 1$ Oe at a frequency f_p, we obtain $\beta_E \approx 1.55$ V/(cm Oe). For the nonlinear direct ME effect, the efficiency of generating the subharmonic with half frequency can be characterised as $\beta_E^{(0.5)} = v_s / (a_p h)$. Using the results of Figs 5-7 for large amplitudes of magnetic pump field ($h \approx 5$ Oe) we have got $\beta_E^{(0.5)} \approx 0.27$ V/(cm Oe). This value is approximately ~6 times smaller than the coefficient for the linear direct ME effect.

For the converse ME effect, the efficiency of generating the subharmonic with half frequency can be characterised by parameter $\beta_B^{(0.5)} = \delta B / e$, where δB is the amplitude of change in induction of the FM layer at frequency f_s that is caused by field e with frequency f_p. The change in induction

can be found from the Faraday's electromagnetic induction law $\delta B = v/(NS2\pi f_s)$, where S is the cross section of the FM layer. For the experimental results shown in Figs 8-10, where the maximum amplitude is $v_s \approx 4.5$ mV at $f_s \approx 4.8$ kHz, and for the sample parameters N_1=200 and $S \approx 3\cdot10^{-7}$ m^2, we obtained $\delta B \approx 13$ G. This gives $\beta_B^{(0.5)} \approx 2.5\cdot10^{-2}$ G/(V/cm) for the maximum efficiency of generation the subharmonic with a half frequency for the converse ME effect. This value is also approximately one order of magnitude smaller than the coefficient for the linear converse ME effect in the same structure.

For the transformer regime, the maximum efficiency of generation the subharmonic with half frequency, as follows from the data presented in Figs 11-13, is $\beta_E^{(0.5)} = v_s/(a_p h) \approx 1.2\cdot10^{-2}$ V/(cm Oe), i.e. approximately ~2 orders of magnitude smaller than for the linear direct ME effect.

Note that generation of the subharmonic in all three regimes begins at relatively small threshold fields: $h_{th} \approx 2$ Oe and $e_{th} \approx 50$ V/cm, which are easy to produce. This suggests that parametric processes should be easily observable and should be highly common in various composite structures and single-phase multiferroics [37,38].

VI. CONCLUSION

In this work, we experimentally observed and investigated parametric generation of the half-frequency subharmonic in a disk composite multiferroic resonator, containing a layer of amorphous ferromagnet that is mechanically coupled to a layer of piezoelectric. The generation of the subharmonic was observed in three different regimes: (i) in the direct ME effect regime, by excitation of the resonator with a harmonic magnetic field; (ii) in the converse ME effect regime, by excitation with a harmonic electric field and (ii) in the transformer regime. An excitation of the resonator by magnetic or electric field with a frequency close to the bending acoustic mode of the resonator, a subharmonic with half frequency that is close to the frequency of another mode of bending oscillations of the structure is generated. The generation occurs for excitation fields in a limited range of frequencies and is of a threshold nature. The amplitude of the generated signal is a nonlinear function of both the excitation field amplitude and the magnitude of tangential component of the static magnetic field. The parametric generation occurs due to the magneto-acoustic nonlinearity of the ferromagnetic layer of the resonator, resulting in an interaction of the acoustic modes. A theory has been developed that qualitatively describes the main characteristics of the subharmonic generation in composite multiferroic resonators.

ACKNOWLEDGEMENTS

The work was supported by the Russian Foundation for Basic Research, projects No 19-07-00594\19 and No 18-52-16001. A universal setup for studying ME effects was created as part of the Russian Science Foundation project No 17-12-01435-P. Some measurements were performed on the equipment of the Joint Collective Use Center of RTU MIREA.

Corresponding author: fetisov@mirea.ru

[1]J.F. Scott, Applications of magnetoelectrics, J. Mater. Chem. **22**, 4567 (2012).
[2]Y. Wang, J. Li, D. Viehland, Magnetoelectrics for magnetic sensor applications: status, challenges and perspectives, Materials Today **17**, 269 (2014).
[3]S. Marauska, R. Jahns, H. Greve, E. Quandt, R. Knochel, B. Wagner, MEMS magnetic field sensor based on magnetoelectric composites, J. Micromech. Microeng. **22**, 065024 (2012).
[4]G. Srinivasan, Y.K. Fetisov, Ferrite-piezoelectric layered structures: Microwave magnetoelectric effects and electric field tunable devices, Ferroelectrics **342**, 65 (2006).
[5]J. Lou, D. Reed, M. Liu, N.X. Sun, Electrostatically tunable magnetoelectric inductors with large inductance tunability, Appl. Phys. Lett. **94**, 112508 (2009).
[6]T. Nan, H. Lin, Y. Gao et al, Acoustically actuated ultra-compact NEMS magnetoelectric antennas, Nature Comm. **8**, 296 (2017).
[7]J.M. Hu, L.Q Chen, C.W. Nan, Multiferroic heterostructures integrating ferroelectric and magnetic materials, Adv. Mater. 28, 15 (2016).
[8]A.A. Klimov, N. Tiercelin, Y. Dusch et al, Magnetoelectric write and read operations in a stress-mediated multiferroic memory cell, Appl. Phys. Lett. **110,** 222401 (2017).
[9]J. Shen, J. Cong, D. Chang, Y. Chai, S. Shen, K. Zhai, Y. Sun, A multilevel nonvolatile magnetoelectric memory, Sci. Rep. **6**, 34473 (2016).
[10]S. Priya, J. Ryu, C. S. Park, J. Oliver, J.J. Choi, D.S. Park, Piezoelectric and magnetoelectric thick films for fabricating power source in wireless sensor nods, Sensors **9**, 6362 (2009).
[11]J. Van Suchtelen, Product properties: a new application of composite materials, Philips Res. Rep. **27**, 28 (1972).
[12]C.W. Nan, M.I. Bichurin, S. Dong, D. Viehland, G. Srinivasan, Multiferroic magnetoelectric composites: historical perspective, status, and future directions, J. Appl. Phys. **103,** 031101 (2008).
[13]M.M. Vopson, Y.K. Fetisov, G. Caruntu, G. Srinivasan, Measurement techniques of the magnetoelectric coupling in multiferroics, Materials **10**, 963 (2017).
[14]H. Palneedi, V. Annapureddy, S. Priya, J. Ryu, Status and perspectives of multiferroic magnetoelectric composite materials and applications, Actuators **5**, 9 (2016).
[15]S.V. Saveliev, L.Y. Fetisov, D.V. Chashin, P.A. Shabin, D.A. Vyunik, F.A. Fedulov, W. Kettl, M. Shamonin, Method of measuring deformations of magnetoactive elastomers under the action of magnetic fields, Rus. Techn. J. **7**, 81 (2019).
[16]Z. Chen, Y. Su, S.A. Meguid, The effect of field-orientation on the magnetoelectric coupling in Terfenol-D/PZT/Terfenol-D laminated structure, J. Appl. Phys. **116**, 173910 (2014).
[17]H. Yao, Y. Shi, Y.W. Gao, A two-dimensional model for magnetic-field-direction dependent magnetoelectric effect in laminated composites, J. Appl. Phys. **118**, 234104 (2015).
[18]M. Bichurin, D. Filippov, V. Petrov, V. Laletsin, N. Paddubnaya, G. Srinivasan, Resonance magnetoelectric effects in layered magnetostrictive-piezoelectric composites, Phys. Rev. B. **68**, 132408 (2003).
[19]V.M. Petrov, G. Srinivasan, M.I. Bichurin, T.A. Galkina, Theory of magnetoelectric effect for bending modes in magnetostrictive-piezoelectric bilayers, J. Appl. Phys. **105**, 063911 (2009).
[20]C. Kirchhof, M. Krantz, I. Teliban, R. Jahns, S. Marauska, B. Wagner, R. Knochel, M. Gerken, D. Meyners, E.

Quandt, Giant magnetoelectric effect in vacuum, Appl. Phys. Lett., **102**, 232905 (2013).
[21]K.E. Kamentsev, Y.K. Fetisov, G. Srinivasan, Low-frequency nonlinear magnetoelectric effects in a ferrite-piezoelectric multilayer, Appl. Phys. Let. **89,** 142510 (2006).
[22]L.Y. Fetisov, D.V. Chashin, D.A. Burdin, D.V. Saveliev, N.A. Ekonomov, G. Srinivasan, Y.K. Fetisov, Nonlinear converse magnetoelectric effects in a ferromagnetic-piezoelectric bilayer, Appl. Phys. Lett. **113**, 212903 (2018).
[23]L. Shen, M. Li, J. Gao et al, Magnetoelectric nonlinearity in a magnetoelectric laminate sensors, J. Appl. Phys. **110**, 114510 (2011).
[24]D.A. Burdin, D.V. Chashin, N.A. Ekonomov, Y.K. Fetisov, L.Y. Fetisov, G. Sreenivasulu, G. Srinivasan, Resonance mixing of alternating current magnetic fields in a multiferroic composite, J. Appl. Phys. **113**, 033902 (2013).
[25]D.V. Saveliev, Y.K. Fetisov, D.V. Chashin, L.Y. Fetisov, D.A. Burdin, N.A. Ekonomov, Magnetoelectric effects in a layered ferromagnet-electrostrictor heterostructure J. Magn. Mag. Mater. **466**, 219 (2018).
[26]D.A. Burdin, D.V. Chashin, N.A. Ekonomov, L.Y. Fetisov, Y.K. Fetisov, Suppression of nonlinear magnetoelectric effect hysteresis in a layered ferromagnetic-piezoelectric structure, J. Magn. Mag. Mater. **449**, 152 (2018).
[27]Y.K. Fetisov, D.A. Burdin, N.A. Ekonomov et al, Bistability in a multiferroic composite resonator, Appl. Phys. Lett. **113**, 022903 (2018).
[28]Y. Wang, T.-D. Onuta, C.J. Long, Y. Cheng, I. Takeuchi, Colossal magnetoelectric effect induced by parametric amplification, Appl. Phys. Lett. **107**, 192902 (2015).
[29]D.A. Burdin, D.V. Chashin, N.A. Ekonomov, Y.K. Fetisov, Parametric amplification of magnetoacoustic oscillations in a ferromagnet-piezoelectric structure, Techn. Phys. Lett. **46**, 201 (2020).
[30]S.A. Akhmanov, R.V. Khokhlov. *Problems of nonlinear optics* (Gordon and Breach Science Publishers, 1973).
[31]R. L. Comstock, R. C. LeCraw, Instability of elastic waves by time-varying elastic modulus in ferromagnets, Phys. Rev. Letts. **10**, 219 (1963).
[32]V.I. Ozhogin, V.L. Preobrazhenskii, Anharmonicity of mixed modes and giant acoustic nonlinearity of antiferromagnets, Sov. Phys. Usp. **31**(8) 713 (1988).
[33]Metglas®, Inc.: www.metglas.com
[34]Elpa Research Institute: www.elpapiezo.ru
[35]S. Timoshenko, *Vibration problems in engineering* (D. Van Nostrand Company, Inc, Toronto, 1955).
[36]V.I. Ozhogin, V.L. Preobrazhensky, Nonlinear dynamics of coupled systems near magnetic phase transitions of the "order-order" type, J. Magn. Magn. Mater. **100**, 554 (1991).
[37]L. Qiao, X. Bi, Evaluation of magnetoelectric coupling in BaTiO3-Ni composite ferroic film by impedance spectroscopy, Appl. Phys. Lett. **91**, 214101 (2008).
[38]J.F. Scott, Room-temperature multiferroic magnetoelectrics, NPG Asia Materials. **5**, e72 (2013).

CAPTIONS FOR FIGURES

FIG. 1. Schematic diagram of the FM-PE resonator with excitation and receiving coils subjected to a static magnetic field *H*.

FIG. 2. Block diagram of the setup for studying parametric generation upon excitation of the resonator by magnetic field.

FIG. 3. Amplitude-frequency (a) and phase-frequency (b) responses of FM-PE resonator for h = 1 Oe and H = 18 Oe.

FIG. 4. Frequency spectra of generated voltage due to direct ME effect for H = 18 Oe, when: (a) field h = 1 Oe is below threshold; (b) field h = 4 Oe is above threshold.

FIG. 5. Subharmonic amplitude as a function of pump field frequency for direct ME effect and different amplitudes of alternating magnetic field h in static field H = 45 Oe.

FIG. 6. Subharmonic amplitude as a function of static field for direct ME effect for different pump field amplitudes h and f_p = 9.7 kHz.

FIG. 7. Dependences of subharmonic amplitude on amplitude of excitation field for f_p = 9.7 kHz and different static fields H in the case of direct ME effect.

FIG. 8. Subharmonic amplitude vs pump field frequency at H = 30 Oe and different amplitudes of field e in the case of converse ME effect.

FIG. 9. Subharmonic amplitude as a function of static magnetic field for pump frequency f_p = 9.7 kHz and different amplitudes of alternating electric field e in the case of converse ME effect.

FIG. 10. Subharmonic amplitude as a function the excitation field amplitude for f_p = 9.7 kHz and different magnetic fields H in the case of converse ME effect.

FIG. 11. Subharmonic amplitude vs pump frequency for different amplitudes of alternating magnetic field and H =25 Oe measured in the transformer regime.

FIG. 12. Subharmonic amplitude vs static magnetic field for different pump field amplitudes at frequency f_p = 9.7 kHz measured in the transformer regime.

FIG. 13. Subharmonic amplitude as a function the excitation field amplitude at f_p=9.7 kHz for different fields H measured in the transformer regime.

FIG. 14. Dependences of subharmonic intensity on normalized pump frequency for different supercriticality levels when the pump frequency is tuned to the mechanical resonance.

FIG. 15. Dependences of subharmonic intensity on normalized pump frequency for different supercriticality levels in the case of mismatch between pump and resonance frequencies.

FIG. 16 Dependences of subharmonics intensity on level of supercriticality for different mismatches between doubled frequency of the subharmonic mode and frequency of the pump mode.

FIG 17 Dependence of magnetostriction λ and piezomagnetic module $\lambda^{(1)}$ on static magnetic field H for the FeBSiC layer.